Vol. 35 No. 145 Journal of the Communications Research Laboratory July 1988
Printed in Tokyo, Japan pp. 163–181

A FEASIBILITY STUDY OF RAIN RADAR FOR THE TROPICAL RAINFALL MEASURING MISSION
5. Effects of Surface Clutter on Rain Measurements from Satellite

By
Takeshi MANABE and Toshio IHARA

(Received on April 25, 1988)

ABSTRACT

As a part of the feasibility study of the satellite-borne rain radar for the Tropical Rainfall Measuring Mission (TRMM), quantitative estimation of the effects of surface clutter on rain measurement is made for clutter coming from sea surface. The sea-clutter interference discussed here includes that entering through the pulse-compression range sidelobe and that through the antenna sidelobe. Calculations are made for the proposed dual-frequency radar operating at 13.8 and 24.15 GHz. It is found that sea clutter received through the range sidelobe can considerably interfere with rainfall measurements up to several mm/h at 13.8 GHz, while interference through the antenna sidelobe is not so significant, only affecting the measurements of very weak rainfall below several tenths of mm/h.

1. Introduction

In rain observation with satellite-borne rain radar, one important problem is to clarify the effects of surface clutter. Surface clutter is unwanted backscattering echo from land or sea surface, which may interfere with the rain observation by acting as background noise. In the worst case it blacks out the rain echo, because backscattering cross sections of land or sea surfaces are much larger than that of rain. Two different interference schemes by which surface clutter impinges upon rain echo should be considered in the feasibility study of the TRMM rain radar: one is interference through the range sidelobe, and the other is interference through the antenna sidelobe. The former is peculiar to the pulse-compression radar system as described in Ref. (1), while the latter is common to both pulse-compression and non-pulse-compression radar systems whose antenna-sidelobe levels are not low enough.

In this paper, the effects of surface clutter on rain measurements by the dual-frequency TRMM rain radar operating at 13.8 and 24.15 GHz are quantitatively evaluated for interferences through both range sidelobe and antenna sidelobe. The most awaited data expected from the TRMM mission is the rain data from over tropical oceans, because they cannot be covered by conventional surface-based observations. Therefore, the case studies in this paper focus the discussion on the effects of sea clutter. The assumed system parameters of the rain radar and the models of rain and sea surface employed in the present studies are described in Section 2. The results of the quantitative analysis of the effects of sea clutter on rain measurements for interferences through range sidelobe and antenna sidelobe are discussed in Section 3 and 4, respectively. For simplicity, we treated the two interference schemes separately although they may coexist in the pulse-compression radar system.

2. Basic Assumptions

2.1 Radar System

The radar system parameters assumed in the following case studies are listed in Table I. A dual-frequency radar at 13.8 and 24.15 GHz is assumed to operate from a satellite at an altitude of 320 km above the surface of the earth. A pulse-compression mode of operation with a compressed pulse width of 0.333 μs is assumed. The range resolution achieved by this pulse-compression mode is 50 m per individual compressed pulse before range integration. The dependence of the antenna gain and the beamwidth on the scanning angle of the electronic scanning antenna is ignored, since, for scanning angles smaller than 20°, their effects are considered to be less than 0.3 dB which is negligible compared with the large errors introduced by the uncertainty of the sea surface model described below.

Table I. Assumed radar system parameters.

Frequency	13.8 GHz	24.15 GHz
Antenna		
Gain	47.5 dB	47.5 dB
Beamwidth	0.76° x 0.76°	0.76° x 0.76°
Transmit Power	48.5 W	32.0 W
Pulse Width	50 μs	50 μs
Compressed Pulse		
Peak Power	7.3 kW	4.8 kW
Compressed Pulse Width	0.333 μs	0.333 μs
Satellite Altitude	320 km	320 km

2.2 Model of Rain

A spatial structure of rain is assumed as follows: a uniform rain region extends from the surface to the rain top 5 km above the surface; the rain top is covered by a bright band 0.5 km thick; scattering and attenuation due to hydrometeors above the bright band are ignored.

The average radar return power from rain is proportional to the radar reflectivity η given by

$$\eta = \int_0^\infty \sigma(D)\, N(D)\, dD, \quad (1)$$

where $\sigma(D)$ is the radar cross section of a raindrop with diameter D, and $N(D)dD$ is the number density of raindrops with diameters in the interval between D and $D + dD$ per unit volume. The radar reflectivity η is related to the equivalent reflectivity factor Z_e by

$$\eta = (\pi^5/\lambda^4)\, |\kappa|^2 Z_e, \quad (2)$$

where $\kappa = (\epsilon - 1)/(\epsilon + 2)$, ϵ is the complex permittivity of water, and λ is the radar wavelength. In the Mie scattering region, Z_e depends on wavelength, raindrop temperature, dropsize distribution, and rainfall rate R. The Z_e-R relationship is known empirically to be approximated by a power-law relation in the form

$$Z_e = \alpha R^\beta. \quad (3)$$

The Z_e-R and η-R relationship used in the present study are listed in Table II. The Z_e-R relationship at 13.8 GHz shown in Table II is based on the empirical fits of the Joss experimental data supplied by Ulbrich[2]. On the other hand, the relationship at 24.15 GHz is obtained by the regression to the Mie calculations for the Marshall-Palmer distribution[3] of 0°C raindrops*.

The attenuation coefficient of rain α_R is also dependent on wavelength, raindrop temperature, dropsize distribution, and rainfall rate, and its dependence on rainfall rate is approximated by a power-law relation in the form[5]

$$\alpha_R = aR^b \quad \ldots\ldots (4)$$

The α_R-R relationships used in the present study are listed in Table II. The α_R-R relationship at 13.8 GHz shown in Table II is based on the parameters a and b tabulated by Olsen

Table II. Radar reflectivities and attenuation coefficients.

Frequency	13.8 GHz	24.15 GHz
Z_e (mm^6/m^3)	$372.4\,R^{1.54}$ †	$278.0\,R^{1.43}$ ††
$\lvert K \rvert^2$	0.9255	0.9076
η (m^{-1})	$4.757 \times 10^{-7} R^{1.54}$	$3.266 \times 10^{-6} R^{1.43}$
α_R (dB/km)	$0.032\,R^{1.124}$ §	$0.0897\,R^{1.106}$ §§

† Ulbrich[2]
†† Marshall-Palmer distribution (0°C)[4]
§ Marshall-Palmer distribution (0°C)[2]
§§ Marshall-Palmer distribution (10°C)[4]

et al.[5] for the Marshall-Palmer distribution of 0°C raindrops interpolated to 14 GHz[2]. On the other hand, the relationship at 24.15 GHz is obtained by the regression to the Mie calculations for the Marshall-Palmer distribution of 10°C raindrops*.

The bright band is a thin layer just below the 0°C isotherm where the melting of falling snow occurs. Although details are still unknown, the attenuation coefficient of the bright band is assumed in the calculations to be twice as large as that of the rain region below.

Besides the rain attenuation, the radar wave suffers the attenuation due to atmospheric gaseous absorption. However, the two-way total attenuation is very small (much less than 1 dB at both frequencies even for the farthest range). Furthermore, the effect of gaseous absorption is almost cancelled out when the power ratio of rain echo to surface clutter is in question, because the interfered rain echo and the interfering surface clutter travel almost the same distance through the atmosphere. Therefore, the effect of atmospheric gaseous absorption is ignored in the examination.

* As has been pointed out by Olsen et al.[5], the Marshall-Palmer distribution, though parametrized by rainfall rate, does not satisfy the rainfall-rate integral equation. The power-law relationships at 24.15 GHz used in the present study are derived by regressions in terms of the rainfall rate given by the rainfall-rate integral assuming the Gunn and Kinzer spectrum of raindrop terminal velocity[4].

2.3 Scattering Property of Sea Surface

The scattering property of sea surface relevant to the estimation of sea clutter is characterized by the normalized radar cross section σ^0 defined as the backscattering coefficient per unit area of sea surface. The normalized radar cross section σ^0 depends on the sea surface condition, the radio frequency, and the angle of incidence. Provided that the sea surface is an isotropic random rough surface with Gaussian statistics, the dependence of σ^0 on the angle of incidence Θ is expressed for small angles of incidence ($\Theta < 20^\circ$) as

$$\sigma^0(\Theta) = \sigma^0(0)\sec^4\Theta\exp\left(-\frac{\tan^2\Theta}{S^2}\right), \quad \cdots\cdots\cdots\cdots\cdots\cdots\cdots\cdots \quad (5)$$

on the basis of the Kirchhoff model under the stationary-phase approximation[6]. In Eq.(5), S is the total variance of surface slopes.

Only a very few experimental data are available on the radar cross section of sea surface at frequencies around 14 or 24 GHz. Figure 1 shows experimental data of $\sigma^0(\Theta)$ of sea

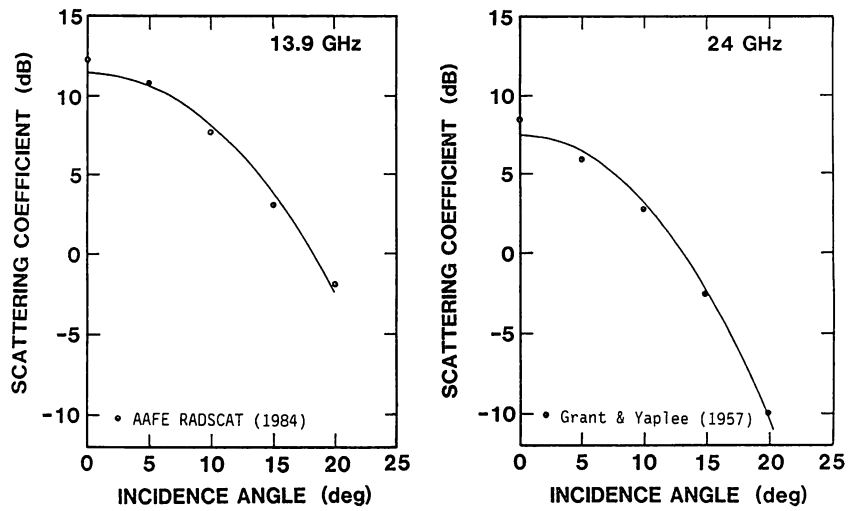

Fig. 1. Backscattering cross section of sea surface as a function of the angle of incidence
⊛ : Experimental data
— : Best-fit curves given by Eq.(5) and Table III.

surface for vertical polarization obtained by the AAFE RADSCAT flight experiment at 13.9 GHz for wind speeds between 7.5 and 10 m/s[7] and by Grant and Yaplee at 24 GHz for a wind speed of 7.5 m/s[8]. These experimental data are approximated by Eq.(5) by applying the least-squares method for angles of incidence between 0 and 20° at each frequency as depicted by solid lines in Fig. 1. The best-fit values of the parameters $\sigma^0(0)$ and S are shown in Table III. These approximated cross sections given by Eq.(6) with the parameters given in Table III are used throughout the following calculations.

Table III. Parameters of sea-surface backscattering coefficient.

	13.9 GHz	24 GHz
$\sigma^0(0)$	14.14 (11.51 dB)	5.62 (7.52 dB)
S	0.1959	0.1744

3. Sea-clutter Interference Through Range Sidelobe

When the pulse-compression technique is employed, sea clutter may interfere with rain echo through the range sidelobe which precedes the compressed main pulse. Although the actual compressed pulse has a complicated range-sidelobe pattern, as shown in Ref.(1), a simplified model is assumed for the range-sidelobe pattern in the following evaluation. The compressed main pulse has an idealized rectangular envelope with duration τ and peak power P_t. The range sidelobe of the compressed pulse is assumed to extend infinitely with a constant level on both sides of the main pulse. Sea clutter is assumed to interfere with rain echo only through its range sidelobes, while rain echo is carried only by the rectangular main pulse. This assumption may be somewhat oversimplified and becomes erroneous for rain range cells very close to the sea surface. However, it still seems to be acceptable, as a zero-th order approximation, for the worst case evaluation of the sea-clutter interference with the rain echoes at places higher than a few range cells away from the sea surface. Accuracy of the model near the sea surface is not important, because there is no way to prevent the strong sea clutter from seriously contaminating the rain echoes for range cells very close to the sea surface. The effects of the antenna sidelobe are examined separately in the next section.

The observation geometry is illustrated in Fig. 2. The antenna pattern is assumed to be

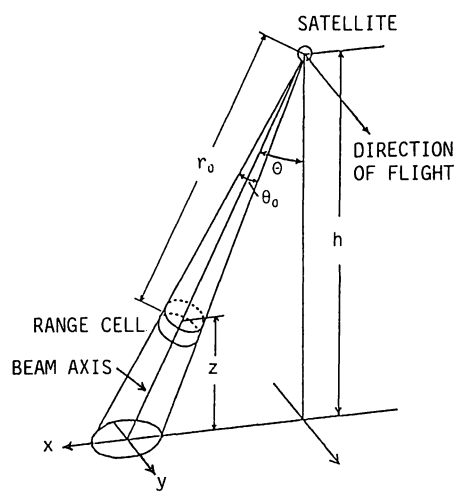

Fig. 2. Geometry for the calculation of the effects of sea-clutter interference through range sidelobe on the measurement of rainfall at range r_0.

Gaussian, and its main-lobe gain pattern is expressed by

$$G = G_0 \exp\left(-\frac{\theta^2 + \phi^2}{\theta_0^2} 4 \ln 2\right), \quad (6)$$

where θ and ϕ are the azimuthal angles taken from the beam axis as in Fig. 2 and θ_0 is the beam full width at half maximum of the main lobe. Both rain echo and sea clutter are received by the antenna main lobe. Sea-clutter interference through the antenna sidelobe coupling, which will be discussed in the next section, is ignored in this section.

The received power of rain echo, P_r, from range r_0 is given by a radar equation as

$$P_r = \frac{\lambda^2 P_t}{(4\pi)^3} \iiint dV \frac{G^2 \eta}{r_0^4} \exp\left(-k \int_0^{r_0} \alpha_R dr'\right), \quad (7)$$

where P_t is the peak power of the compressed pulse and $k = 0.2 \ln 10$. When the length of the compressed-pulse range bin is short enough and the antenna beamwidth is narrow enough, the integral taken over the volume determined by the rectangular range bin and the Gaussian antenna main lobe yields

$$P_r = \frac{\lambda^2 P_t G_0^2 c\tau \theta_0^2}{1024\pi^2 \ln 2\, r_0^2} \eta \exp\left(-k \int_0^{\infty} \alpha_R\, dr'\right), \quad (8)$$

where

$$r_0 = (h - z) \sec\Theta, \quad (9)$$

In Eq.(9), h is the satellite altitude, and z is the altitude of the range bin where the rain measurement is made.

The power of sea clutter, P_s, received through the range sidelobe is given by

$$P_s = \frac{\lambda^2 q P_t}{(4\pi)^3} \iint dS \frac{G^2 \sigma^0}{r^4} \exp\left(-k \int_0^{r} \alpha_R\, dr'\right), \quad (10)$$

where q is the range-sidelobe level relative to the peak level of the compressed main pulse. The transformations from the surface local coordinates (x, y) to the angular coordinates (θ, ϕ) are

$$x = h \tan(\Theta + \theta), \quad (11)$$

$$y = h \sec\Theta \tan\phi, \quad (12)$$

$$dS = dxdy = h^2 \sec\Theta \sec^2(\Theta + \theta) \sec^2\phi\, d\theta d\phi. \quad (13)$$

When the beamwidth is narrow enough ($\theta_0 \ll \Theta$), the surface integral is simplified, by introducing approximate transformations $dS = h^2 \sec^3\Theta\, d\theta d\phi$ and $r = h \sec\Theta$, to the angular integral over the Gaussian beam

$$P_s = \frac{\lambda^2 q P_t G_0^2 \theta_0^2}{512\pi^2 \ln 2 h^2 \sec\Theta} \sigma^0(\Theta) \exp(-k \int_0^{h \sec\Theta} \alpha_R \, dr') \quad \ldots\ldots\ldots\ldots\ldots (14)$$

In the derivation of Eq. (14), σ^0 is assumed to take the constant value $\sigma^0(\Theta)$ within the antenna beam. It should be pointed out that, although Eq.(14) is derived on the assumption that the off-nadir angle Θ is much larger than the beamwidth θ_0, P_s given by Eq.(14) can be shown to be still valid even for nadir observations if 0 is substituted to Θ.

From Eq.(8) and Eq.(14), the power ratio of rain echo to sea clutter is given by

$$\frac{P_r}{P_s} = \frac{c\tau h^2 \eta}{2(h-z)^2 q \sigma^0(\Theta) \sec\Theta} \exp(k\alpha_R \, z \sec\Theta) \quad \ldots\ldots\ldots\ldots\ldots\ldots\ldots (15)$$

Calcultions of the P_r/P_s ratio were made for a constant range-sidelobe level −50 dB, i.e., $q = 10^{-5}$, using the system parameters for the dual-frequency pulse-compression radar given in Table I. In Figs. 3 – 12, contours of the combinations of altitude z and rainfall rate which give constant P_r/P_s ratios are shown for every 5 dB for off-nadir angles of 0, 5, 10, 15, and 20 degrees. The 0-dB contours are highlighted by thick lines. Given a threshold level of the P_r/P_s ratio above which rain measurement is possible, the range of measurable rainfall rates at an arbitrary altitude can be derived from those contour maps.

It is found that the interference from the sea clutter through range sidelobe limits the radar observation of rainfall at 13.8 GHz, in particular for relatively weak rain up to several mm/h and for small off-nadir observation angles, if the threshold level of the P_r/P_s ratio required for the rain measurement is 0 dB. On the other hand, at 24.15 GHz, the effects

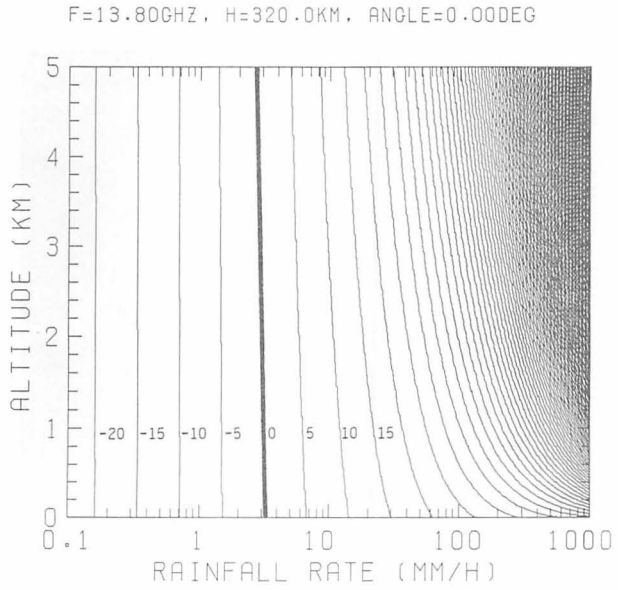

Fig. 3. Contour map of P_r/P_s ratio in dB for sea clutter through range sidelobe at 13.8 GHz for scan angle $\Theta = 0°$.

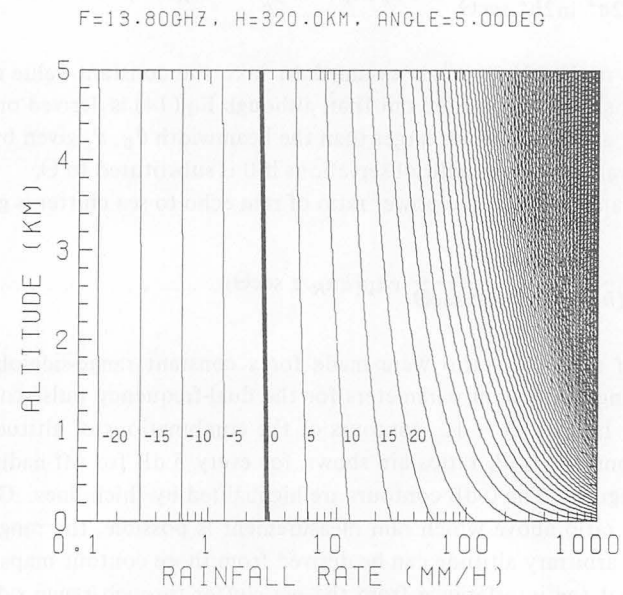

Fig. 4. Contour map of P_r/P_s ratio in dB for sea clutter through range sidelobe at 13.8 GHz for scan angle $\Theta = 5°$.

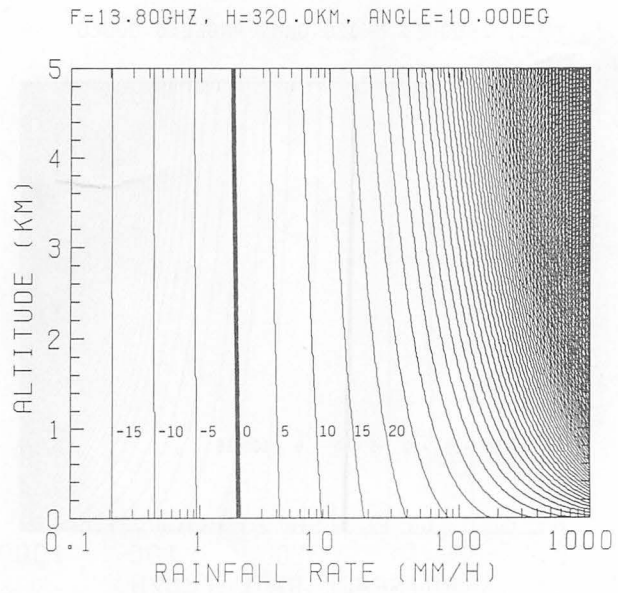

Fig. 5. Contour map of P_r/P_s ratio in dB for sea clutter through range sidelobe at 13.8 GHz for scan angle $\Theta = 10°$.

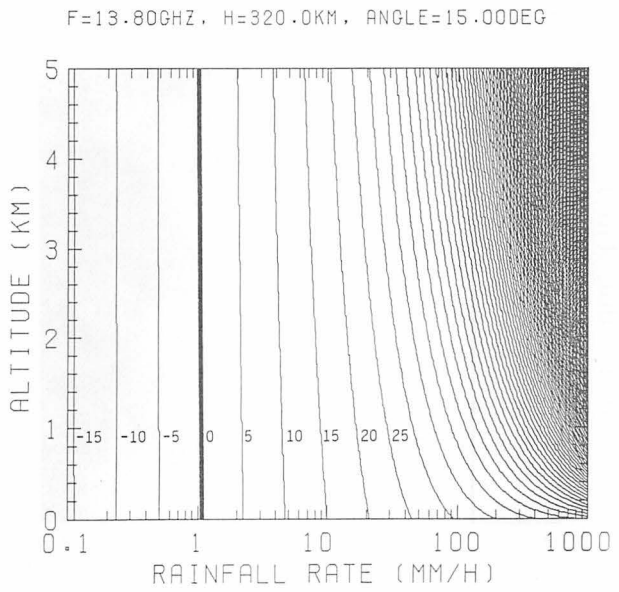

Fig. 6. Contour map of P_r/P_s ratio in dB for sea clutter through range sidelobe at 13.8 GHz for scan angle $\Theta = 15°$.

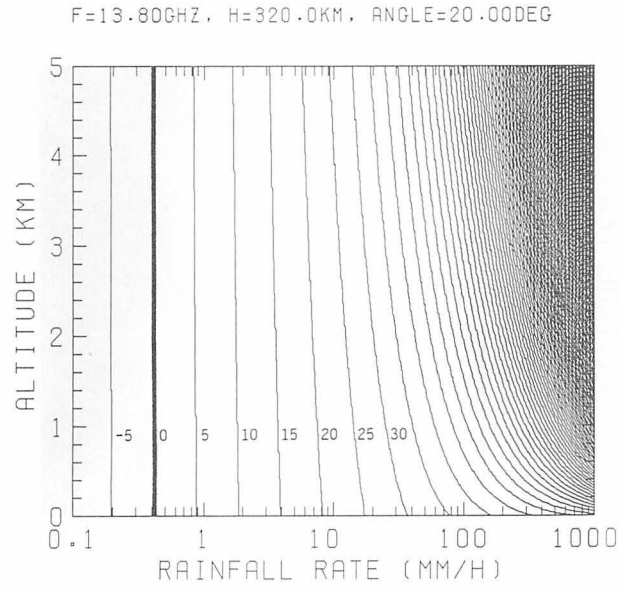

Fig. 7. Contour map of P_r/P_s ratio in dB for sea clutter through range sidelobe at 13.8 GHz for scan angle $\Theta = 20°$.

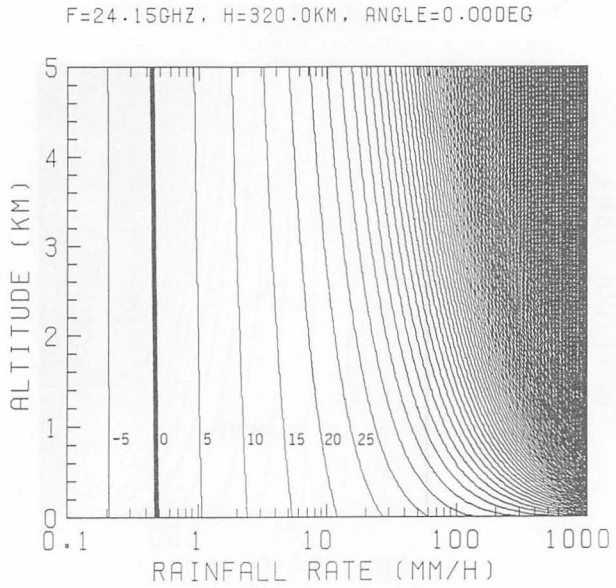

Fig. 8. Contour map of P_r/P_S ratio in dB for sea clutter through range sidelobe at 24.15 GHz for scan angle $\Theta = 0°$.

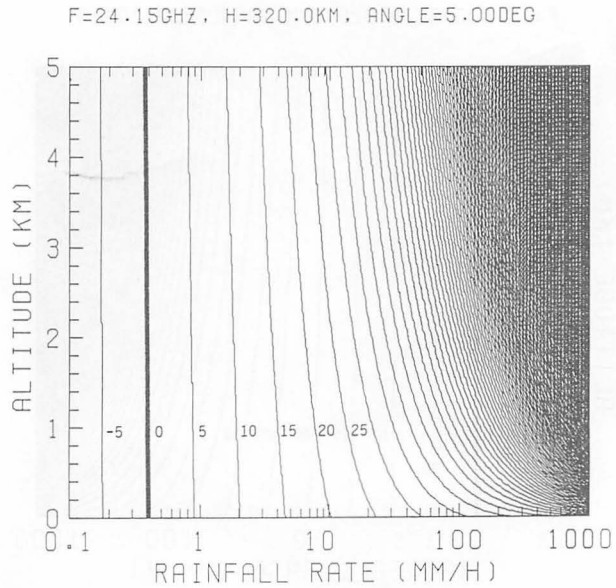

Fig. 9. Contour map of P_r/P_S ratio in dB for sea clutter through range sidelobe at 24.15 GHz for scan angle $\Theta = 5°$.

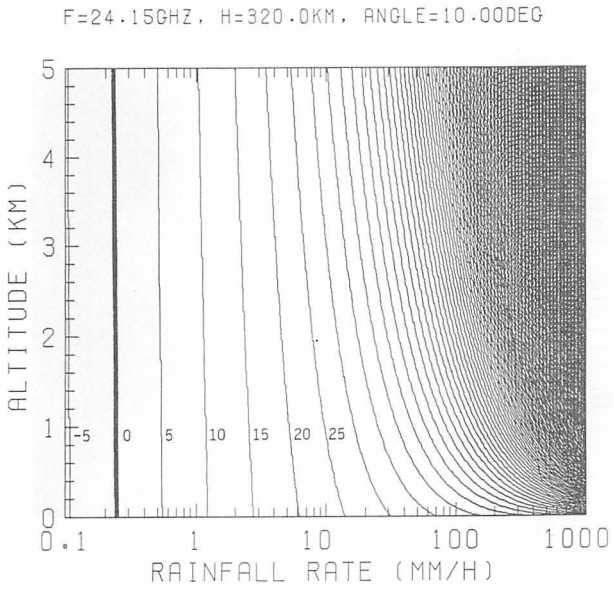

Fig. 10. Contour map of P_r/P_s ratio in dB for sea clutter through range sidelobe at 24.15 GHz for scan angle $\Theta = 10°$.

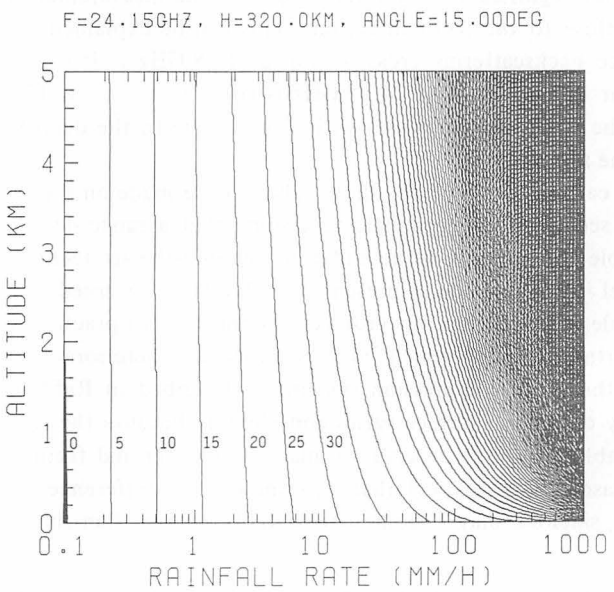

Fig. 11. Contour map of P_r/P_s ratio in dB for sea clutter through range sidelobe at 24.15 GHz for scan angle $\Theta = 15°$.

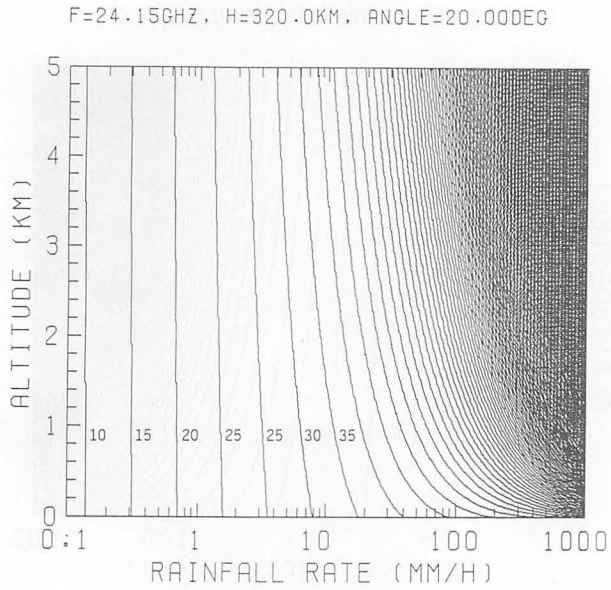

Fig. 12. Contour map of P_r/P_s ratio in dB for sea clutter through range sidelobe at 24.15 GHz for scan angle $\Theta = 20°$.

of sea clutter are less significant, only interfering with the measurement of very weak rain ($R < 0.5$ mm/h) close to the nadir direction. This can be explained by the fact that the assumed sea-surface backscattering cross section at 13.8 GHz is larger than that at 24.15 GHz and the radar reflectivity η at 24.15 GHz is larger than that at 13.8 GHz. For fixed off-nadir angles, the P_r/P_s ratio increases with altitude due to the decrease in rain attenuation suffered by the rain echo.

Although the calculations of P_r/P_s shown above were made on the assumption that $q = 10^{-5}$ (−50 dB), it seems rather optimistic to assume that a range-sidelobe level as low as −50 dB is realizable for satellite-borne radar by state-of-the-art technology. Such a low range-sidelobe level is not possible at present, but should be regarded as a value which may ideally be attainable after another few year's development. For practical satellite operation, there exist uncertain factors which may significantly deteriorate the range-sidelobe characteristics of the pulse compression system, as described in Ref.(1). In addition, the scattering property of the sea surface varies considerably because the sea surface condition may vary appreciably from one observation place to another and from time to time. It is therefore quite reasonable to expect that, in some cases, interference from the sea clutter through the range sidelobe may become considerably severer than shown in Figs. 3 – 12.

4. Interference from the Sea Clutter through the Antenna Sidelobes

When the antenna sidelobe level is not low enough, sea clutter received through the antenna sidelobe may interfere with rain measurements. Figure 13 shows a schematic con-

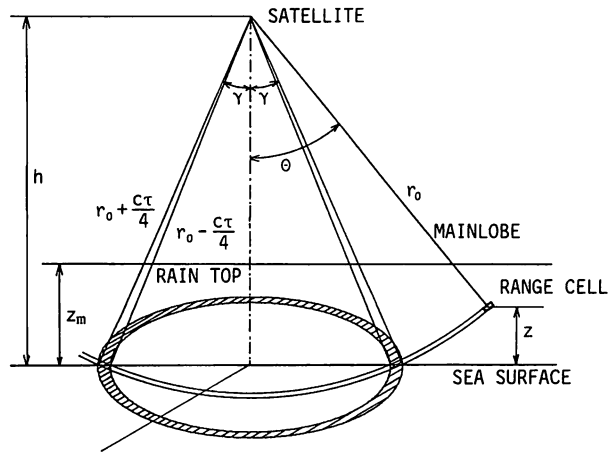

Fig. 13. Geometry for the calculation of the effects of sea-clutter interference through antenna sidelobe on the measurement of rainfall at scan angle Θ and range r_0. The hatched area is the sea surface from which the sea clutter returns through antenna sidelobe.

figuration to illustrate the effects of sea clutter through the antenna sidelobe on rain measurement.

In this section, the radar pulse is assumed to be an idealized rectangular pulse with a duration of τ, free from range sidelobe. If rain echo is assumed to be received only through the Gaussian main lobe given by Eq.(6), rain echo power P_r from rain at range r_0 is given by Eq. (8).

On the other hand, sea clutter is assumed to be received only through the antenna sidelobe, and it is the annular area at the same range r_0 from the satellite on the sea surface, indicated by hatching in Fig. 13, that is responsible for interference with rain echo from range r_0. The power of sea clutter, P_s, from this area is given by a radar equation:

$$P_s = \frac{\lambda^2 P_t}{(4\pi)^3} \iint dS \frac{G_s^2 \sigma^0(\gamma)}{r^4} \exp(-k\alpha_R z_m \sec\gamma), \quad \ldots\ldots\ldots\ldots\ldots\ldots \quad (16)$$

where z_m is the height of the rain region, and the off-nadir angle γ of the sea surface contributing to clutter is given by

$$\gamma = \cos^{-1} \frac{h}{(h - z)\sec\Theta} \quad \ldots\ldots\ldots\ldots\ldots\ldots\ldots\ldots\ldots\ldots\ldots\ldots \quad (17)$$

In Eq. (16), the surface integral is taken over the hatched annular area shown in Fig. 13. Although proper weighting with the squared antenna sidelobe pattern should be applied to calculate the power of sea clutter from this annular area, it is assumed for simplicity that the antenna sidelobe pattern is isotropic with a constant sidelobe gain of G_s. On this assumption, Eq.(16) becomes

$$P_s = \frac{\lambda^2 P_t G_s^2 \sigma^0(\gamma) A}{64\pi^3 (h-z)^4 \sec^4\Theta} \exp(-k\alpha_R z_m \sec\gamma), \quad \cdots\cdots\cdots\cdots\cdots\cdots \quad (18)$$

where A is the area of the hatched annular surface and is given by

$$A = \begin{cases} \pi c\tau (h-z) \sec\Theta, & \text{when } z < h - (h + \frac{c\tau}{4}) \cos\Theta ; \\ \pi\left[\left\{(h-z)\sec\Theta + \frac{c\tau}{4}\right\}^2 - h^2\right], & \text{when } h - (h + \frac{c\tau}{4}) \cos\Theta < z < h - (h - \frac{c\tau}{4}) \cos\Theta; \\ 0, & \text{when } h - (h - \frac{c\tau}{4}) \cos\Theta < z. \end{cases} \quad \cdots\cdots\cdots \quad (19)$$

For a given off-nadir angle Θ, the annular area reduces to a circular area when the altitude z, where the rain observation is made, exceeds $h - (h + c\tau/4)\cos\Theta$, and there exists a critical altitude $[h - (h - c\tau/4)\cos\Theta]$ above which the area vanishes and the rain echo can be observed without sea clutter through the antenna sidelobe.

Calculations of the P_r/P_s ratio were made for a constant antenna sidelobe level of –35 dB, i.e., $G_s/G_0 = 10^{-3.5}$, using the system parameters for the dual-frequency pulse-compression radar given in Table I. Although the first sidelobe level may exceed –30 dB in some cases, as described in Ref. (9), considerable rolloff of sidelobe level justifies the crude assumption of isotropic antenna sidelobe level of –35 dB. In Figs. 14 – 21, contours of the combinations of altitude z and rainfall rate which give constant P_r/P_s ratios are shown for

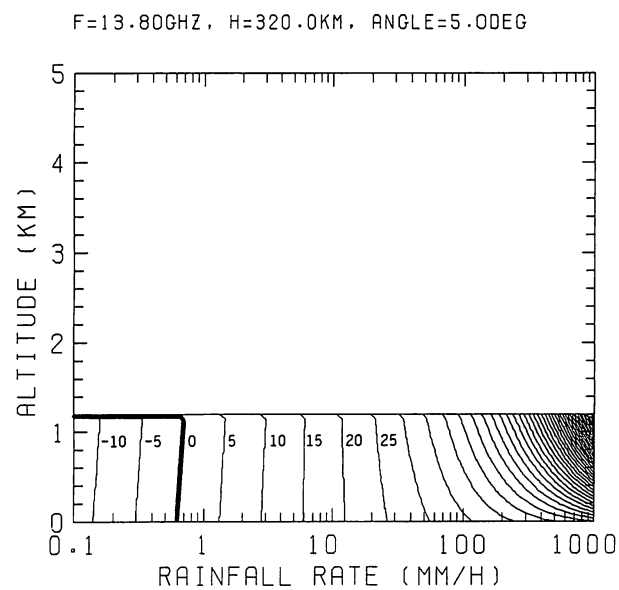

Fig. 14. Contour map of P_r/P_s ratio in dB for sea clutter through antenna sidelobe at 13.8 GHz for scan angle $\Theta = 5°$.

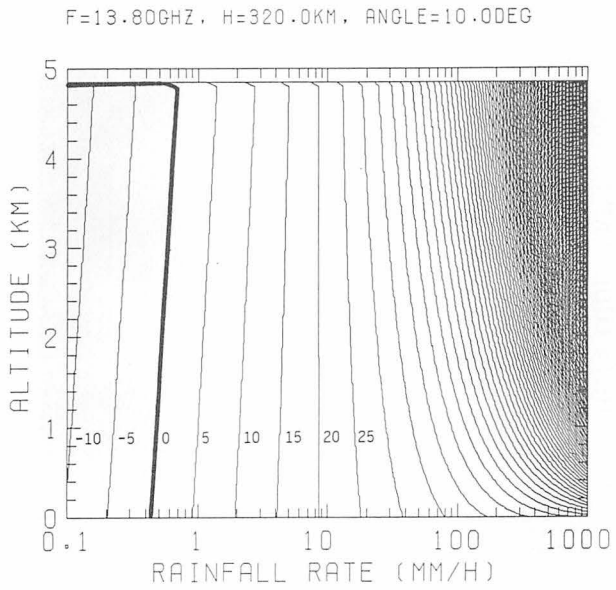

Fig. 15. Contour map of P_r/P_s ratio in dB for sea clutter through antenna sidelobe at 13.8 GHz for scan angle $\Theta = 10°$.

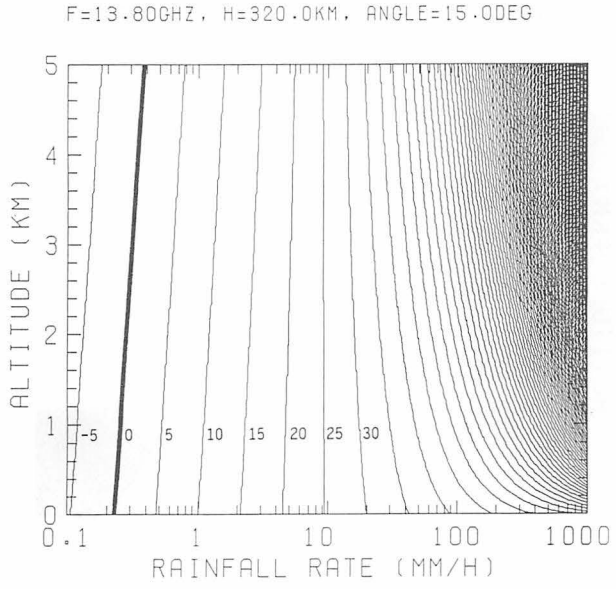

Fig. 16. Contour map of P_r/P_s ratio in dB for sea clutter through antenna sidelobe at 13.8 GHz for scan angle $\Theta = 15°$.

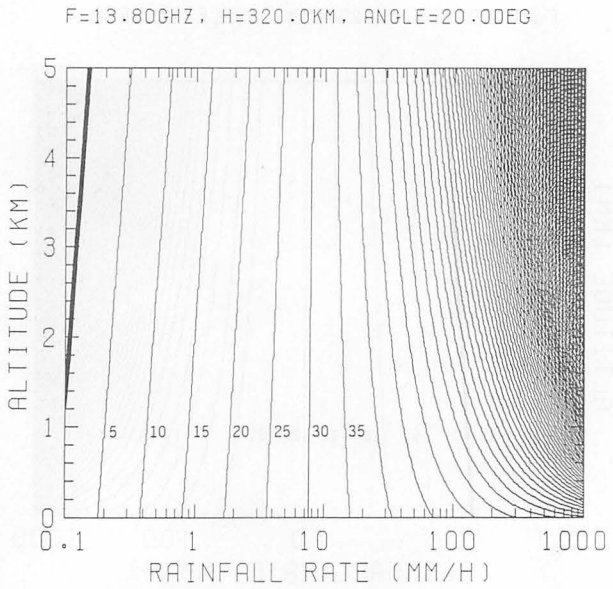

Fig. 17. Contour map of P_r/P_s ratio in dB for sea clutter through antenna sidelobe at 13.8 GHz for scan angle $\Theta = 20°$.

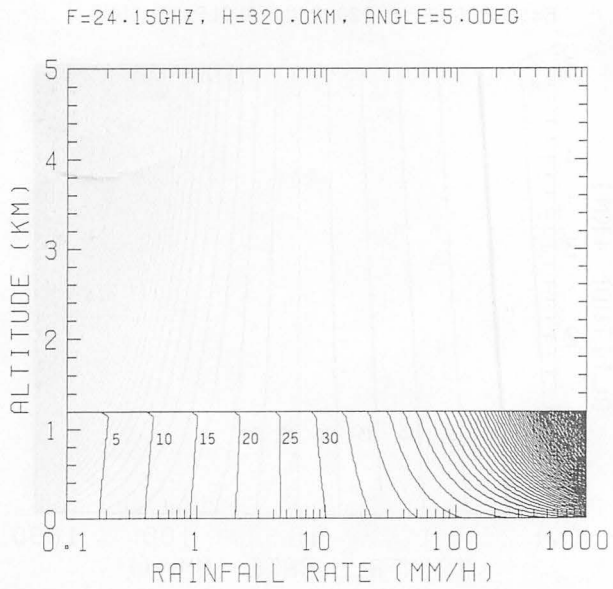

Fig. 18. Contour map of P_r/P_s ratio in dB for sea clutter through antenna sidelobe at 24.15 GHz for scan angle $\Theta = 5°$.

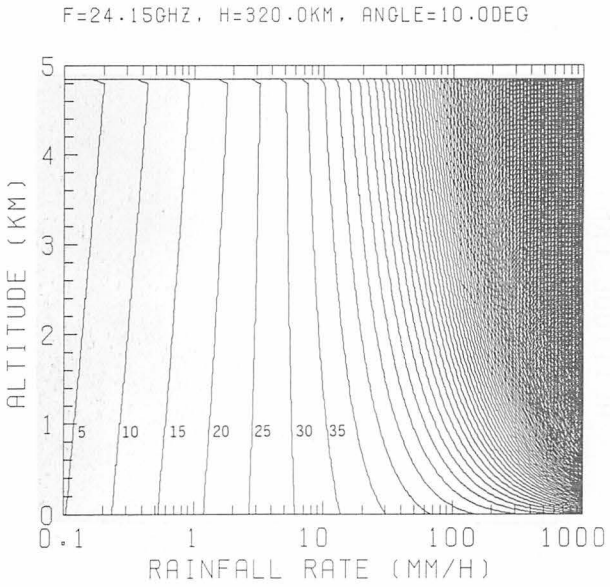

Fig. 19. Contour map of P_r/P_s ratio in dB for sea clutter through antenna sidelobe at 24.15 GHz for scan angle $\Theta = 10°$.

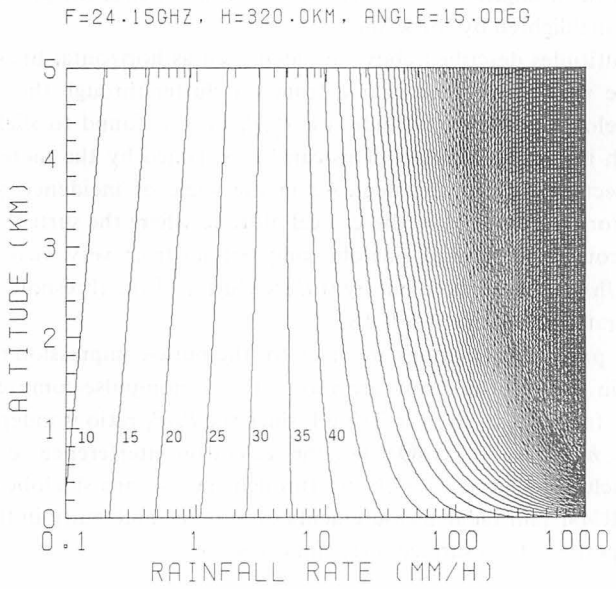

Fig. 20. Contour map of P_r/P_s ratio in dB for sea clutter through antenna sidelobe at 24.15 GHz for scan angle $\Theta = 15°$.

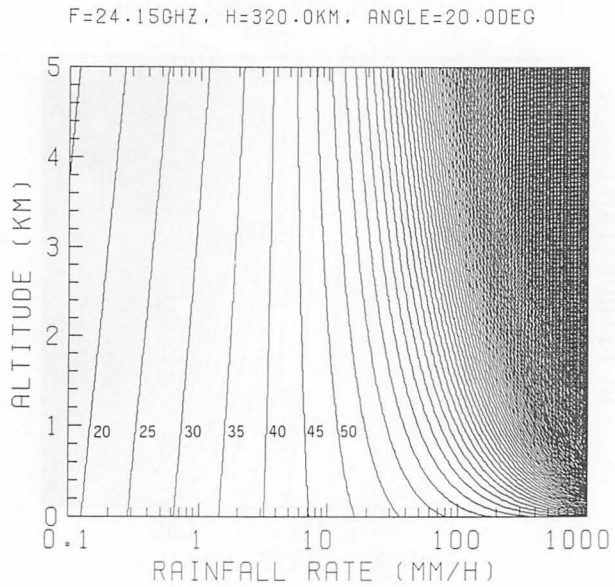

Fig. 21. Contour map of P_r/P_S ratio in dB for sea clutter through antenna sidelobe at 24.15 GHz for scan angle $\Theta = 20°$.

every 5 dB for off-nadir angles of 5, 10, 15, and 20 degrees as in the previous section. The 0-dB contours are highlighted by thick lines.

The critical altitudes described above are identified as horizontal lines in Figs. 14, 15, 18, and 19, above which rain echo is free from sea clutter through the antenna sidelobe, i.e., $P_r/P_S = \infty$. Below the critical altitude, the P_r/P_S ratio is found to slightly decrease, for weak rainfall, with increasing altitude. This can be explained by the increase in sea-surface scattering cross section due to the decrease in the angle of incidence γ with increasing altitude z. Even for altitudes below the critical altitude where the surface clutter interferes with rain echo through the antenna sidelobe, only echoes from very weak rainfall of only a few tenths of mm/h may be blacked out by surface clutter, if the threshold level of the P_r/P_S ratio required for rain measurement is 0 dB.

Although the present calculations are made for the pulse-compression radar with system parameters given in Table I, the results are also useful for non-pulse-compression radars with P_t and τ different from those given in Table I, since the P_r/P_S ratio is independent of P_t and τ for altitudes $z < h - (h + \frac{c\tau}{4}) \cos\Theta$ where the sea-clutter interference becomes significant.

It can be concluded that surface clutter through the antenna sidelobe causes no serious problem in the TRMM rain radar measurements even if the ambiguity in the assumption on the scattering properties of sea surface is taken into account.

5. Concluding Remarks

For the proposed TRMM rain radar operating at 13.8 and 24.15 GHz, the effects of sea clutter entering through the range sidelobe and antenna sidelobe are examined by using the radar equations for rain and clutter. It is found that the sea clutter received through the range sidelobe can seriously interfere with the measurements of weak rainfall. In particular, for near-nadir observation at 13.8 GHz, the level of range-sidelobe sea clutter is as high as that of rain echo for rainfall rate of 3 mm/h. On the other hand, interference through the antenna sidelobe is less significant at both frequencies, only affecting the measurements of very weak rainfall below 0.5 mm/h. Meteorologists require the TRMM rain radar to provide rain data with surface clutter less than the rain echo from rain of 0.5 mm/h for all observation angles and ranges, at both frequencies. The present results seems to be in favor of the non-pulse-compression system rather than the pulse-compression system for the TRMM rain radar as far as sea-clutter interference is concerned.

Although the present examinations are made on the basis of various simplifying models and assumptions, the results may serve as preliminary estimates for the design of the TRMM rain radar.

References

(1) T. Ihara and K. Nakamura; "4. A discussion of the pulse compression and adaptive scanning" J. Commun. Res. Lab., this issue.

(2) K. E. Im, F. Li, D. Rosing, and W. J. Wilson; "Final report – Phase A conceptual design study for a rain radar on the tropical rain mapping mission," Jet Propulsion Laboratory, Pasadena, CA, Feb., 1987.

(3) J. S. Marshall and W. M. K. Palmer; "The distribution of raindrops with size," J. Meteorol., **5**, pp. 165–166, 1948.

(4) T. Kozu, private communication.

(5) R. L. Olsen, D. V. Rogers, and D. B. Hodge; "The aR^b relation in the calculation of rain attenuation," IEEE Trans. Antennas Propagat., **AP-26**, pp. 318–329, 1978.

(6) G. R. Valenzuela; "Theories for the interaction of electromagnetic and oceanic waves – a review," Boundary-Layer Meteorol., **13**, pp. 61–85, 1978.

(7) L. C. Schroeder, W. L. Jones, P. R. Schaffner, and J. L. Mitchell; "Flight measurement and analysis of AAFE RADSCAT wind speed signature of the ocean," NASA Tech. Memo., TM-85646, 1984.

(8) C. R. Grant and B. S. Yaplee; "Back scattering from water and land at centimeter and millimeter wavelengths," Proc. IRE, **45**, 976–982, 1957.

(9) K. Nakamura and T. Ihara; "3. Radar type and Antenna" J. Commun. Res. Lab., this issue.